Chinese Chemical Letters 35 (2024) 108803

Contents lists available at ScienceDirect

Chinese Chemical Letters

journal homepage: www.elsevier.com/locate/cclet

Natural polysaccharide-based smart CXCR4-targeted nano-system for magnified liver fibrosis therapy

Liqiong Sun[a,1], Xinping Luo[b,1], Chenxi Zhou[b], Zhanwei Zhou[b,*], Minjie Sun[b,*]

[a] College of Horticulture, Nanjing Agricultural University, Nanjing 210095, China
[b] NMPA Key Laboratory for Research and Evaluation of Pharmaceutical Preparations and Excipients, State Key Laboratory of Natural Medicines, Department of Pharmaceutics, China Pharmaceutical University, Nanjing 210009, China

ARTICLE INFO

Article history:
Received 16 May 2023
Revised 5 July 2023
Accepted 13 July 2023
Available online 16 July 2023

Keywords:
Nanoparticle
CXCR4 antagonism
ROS-responsive
Hepatic stellate cells
Liver fibrosis

ABSTRACT

Activated hepatic stellate cells (aHSCs), the main source of extracellular matrix deposition, are key targets in liver fibrosis. However, no effective drug specific to aHSCs has been clinically applied due to poor drug delivery efficiency. Herein, we designed a CXC chemokine receptor 4 (CXCR4)-targeted reactive oxygen species (ROS)-responsive platform AMD-Dex-ROS-responsive-sorafenib (ARS) based on natural polysaccharide and thioctic acid frame, which can deliver anti-fibrosis drug represented by sorafenib specifically to aHSCs on account of CXCR4 over-expression on aHSCs, and smartly disassemble *via* ROS-responsive thioketal rupture relying on high intracellular ROS in HSCs, realized on-demand drug release and effective liver fibrosis reversion. Notably, in this platform, the CXCR4 antagonist AMD3100 not only enhanced aHSCs targeting efficiency of sorafenib but also effectively magnified the aHSCs elimination of sorafenib by blocking stroma cell derived factor-1 (SDF-1)/CXCR4-induced aHSCs protection, resulting in synergistic anti-fibrosis effect. The platform provided a new approach for drug delivery system design and liver fibrosis treatment.

Liver fibrosis, precursor of liver cirrhosis and hepatocellular carcinoma (HCC), typical for hindered liver function and expanded extracellular matrix production, essentially collagens, has been a global health problem without approved treatment [1]. As a central contributor to collagen deposition, activated hepatic stellate cells (aHSCs) play a pivotal role in the development of liver fibrosis and represent a potential therapeutic target [2]. In recent study, several therapies proposed for liver fibrosis are promising, among which the most eye-catching one is targeting for aHSCs, including inhibiting their activation or inducing their apoptosis [3].

However, the efficacy of HSC-targeted therapy is hampered by poor drug delivery and complicated microenvironments of the fibrotic liver [4–6], where various cells gathered and regulated the fibrosis process such as Kupffer cells, hepatocytes and liver sinusoidal endothelial cells. According to recent studies [7–9], the tendency of nanoparticles to accumulate in the liver make them ideal candidates for treating liver diseases and the targeting moiety can be decorated on the surface of nanoparticles for targeting specific cells, so the potential of nanoparticles for liver fibrosis treatment was highlighted, but there was still long way to go for efficient drug delivery and clinical application. Designing an elaborate nano-system with higher selectivity specific to aHSCs and intelligent on-demand drug release is still an intractable challenge.

Elevating the selectivity of drug delivery system on HSCs is a crucial strategy for aHSC-targeting therapy [10–12]. CXC receptor 4 (CXCR4) is a transmembrane protein overexpressing on the surface of aHSCs, whose binding with its unique ligand stroma cell derived factor-1 (SDF-1) seriously contributing to HSC activation, fibrogenesis, and proliferation [13–16]. Therefore, introduction of CXCR4 antagonist on the surface of nano-system could not only enhance selectivity on HSCs and at the mean time reduce SDF-1/CXCR4-induced HSC activation and proliferation.

Otherwise, the cytotoxicity of drug on normal hepatocyte or other cells emphasize the urgent need to develop safer system which represents selective drug release [17-19,20]. High reactive oxygen species (ROS) production especially H_2O_2 during liver fibrosis in aHSCs was discovered [21], which plays an important role in the pathogenesis of liver fibrosis, activating redox-sensitive intracellular pathways in HSCs to increase collagen synthesis [22]. The elevated ROS level in aHSCs has the potential to be a sensitive trigger for controlled drug release in pathological microenvironments,

* Corresponding authors.
E-mail addresses: zhouzhanwei0515@163.com (Z. Zhou), msun@cpu.edu.cn (M. Sun).
[1] These authors contributed equally to this work.

https://doi.org/10.1016/j.cclet.2023.108803
1001-8417/

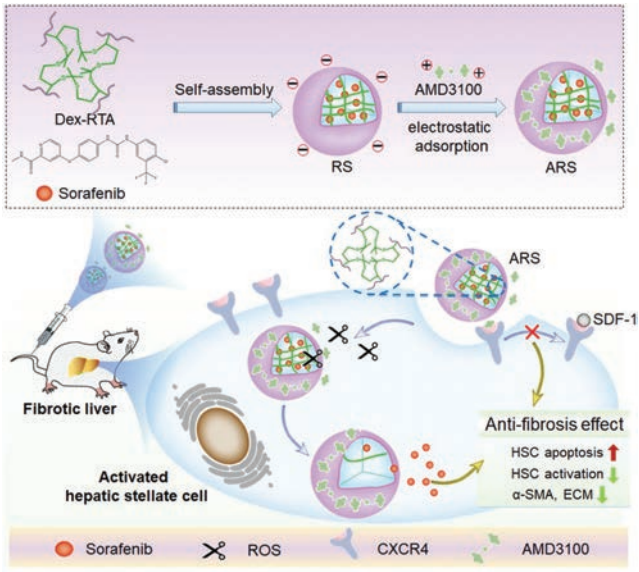

Scheme 1. Schematic illustration of the preparation and the effect mechanism of CXCR4-targeting nano-system based on ROS responsive natural polysaccharide conjugate for amplifying liver fibrosis therapy.

and can therefore be used to develop site-specific drug delivery system [23].

Herein, we designed a multifunctional aHSC-targeting nanoparticle based on natural polysaccharide in order to fully stimulate the anti-fibrotic effect of sorafenib and reduce the unwanted side effect and cytotoxicity (Scheme 1). CXCR4 antagonist AMD3100 served not only as a competitive ligand for targeting aHSCs but also as a therapeutic agent for restraining HSCs activation. In order to reduce unwanted release in other cells, ROS-responsive degradable thioketal group was introduced into the nanoparticles *via* reconstructing natural thioctic acid, contributing to on-demand sorafenib release in high-ROS aHSCs. Above all, a smart delivery system with both targeting and responsive release capabilities was skillfully constructed for magnified liver fibrosis treatment.

Natural polysaccharides are highly biocompatible and universal in nano-system design due to their biosecurity and easily-modified hydroxyl groups [24,25]. So a representative polysaccharide dextran was chosen as a nano-system frame here. First, ROS-responsive amphiphilic conjugate dextran-ROS-responsive thioctic acid derivative (Dex-RTA) was synthesized as described in methods and Fig. S1 (Supporting information). The first step is the reduction of thioctic acid. The presence of the two-SH proton peaks at 1.28 and 1.32 ppm in the ^{1}H nuclear magnetic resonance (NMR) spectroscopic analysis indicated the successful reduction of thioctic acid and the production of the reductive product of thioctic acid dihydro thioctic acid (DHTA) (Fig. S2A in Supporting information). Secondly, the ROS-responsive thioctic acid derivative RTA was synthesized through a condensation reaction of DHTA and 2,2-methylpropane and identified by the presence of thioketal group corresponding to the proton peak at 1.58 ppm (Fig. S2B in Supporting information). Thirdly, the signals at $\delta = 1.75$ ppm (RTA) and $\delta = 4.68$ ppm (anomeric proton in dextran) not only verified the successful synthesis of Dex-RTA but also determined the degree of substitution (DS) of RTA was 55, which was defined as the number of RTA units per 100 anhydroglucosidic (AHG) units (Fig. S2C in Supporting information).

At the same time, the non-ROS-responsive dextran-lauric acid (Dex-LA) which possessed a similar structure with Dex-RTA except for the thioketal group at the end of the hydrophobic substituent was also synthesized by esterification reaction between dextran and lauric acid. The DS of Dex-LA was determined by the anomeric proton in dextran at 4.68 ppm and the $-CH_3$ proton peaks in lauric acid at 0.86 ppm, whose value was 54 similarly as that of Dex-RTA (Fig. S2C).

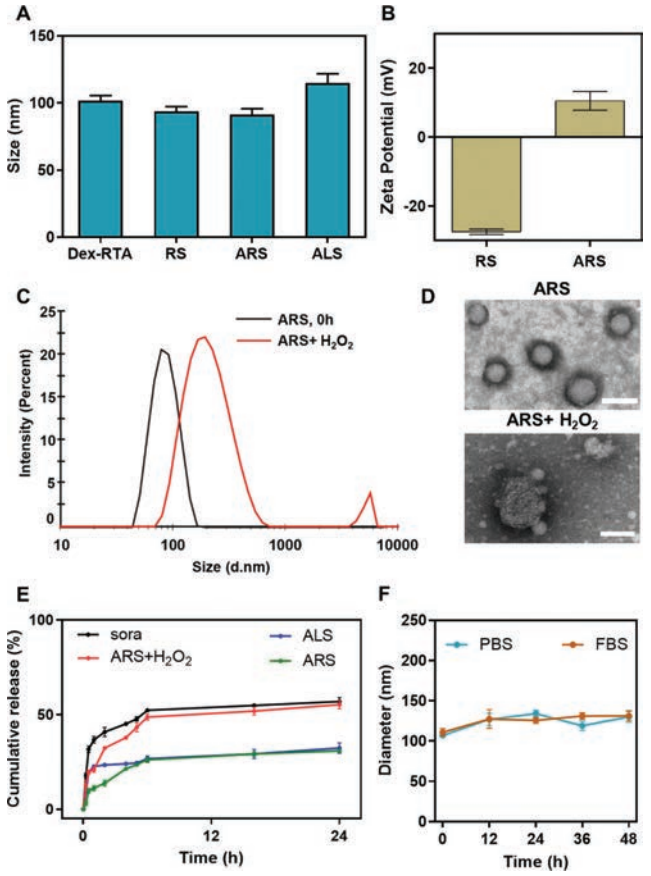

Fig. 1. (A) Particle size of Dex-RTA, RS, ARS and ALS NPs. (B) Zeta potential of RS and ARS NPs. (C) Particle size of ARS NPs before or after 1 mmol/L H_2O_2 treatment. (D) Transmission electron microscope (TEM) images of ARS NPs before or after 1 mmol/L H_2O_2 treatment. Scale bar = 100 nm. (E) Cumulative release of sorafenib after 1 mmol/L H_2O_2 treatment. (F) Size stability of ARS NPs in phosphate buffer solution (PBS) and 10% fetal bovine serum (FBS) solution.

As known, amphiphilic conjugates could self-assemble into nano-sized micelles [26]. So after the synthesis of Dex-RTA and Dex-LA, nano-systems loaded sorafenib were prepared through solvent exchange method, forming Dex-RTA-Sora nanoparticles (RS NPs) and Dex-LA-Sora nanoparticles (LS NPs), respectively. Their particle size was characterized. Sorafenib-loading enhanced the hydrophobic force of hydrophobic core so that the particle size of Dex-RTA-Sora NPs (RS) decreased than Dex-RTA NPs, from 101.80 ± 3.74 nm to 93.74 ± 3.52 nm (Fig. 1A). After AMD3100-adsorption, there was also slight decrease on particle size maybe because the electrostatic interaction between dextran and AMD3100 made the particles more tightly, from 93.74 ± 3.52 nm to 91.28 ± 4.56 nm. What is more, the particle size of ARS nanoparticles was smaller than AMD-Dex-LA-Sora (ALS) nanoparticles, 91.28 ± 4.56 nm and 117.30 ± 3.49 nm, respectively, maybe because the cross-linking of thioketal group made the nanoparticles more tightly. At the same time, absorption of AMD3100 caused a marked charge reversal on the surface of the RS NPs (Fig. 1B), further proving that the positively-charged AMD3100 binds to the negatively-charged surface of the dextran nanoparticles by electrostatic interactions to form AMD-dextran nanoparticles.

Drug loading capacity (DL) and encapsulation efficiency (EE) of sorafenib in ARS NPs was measured and the results showed that the most efficient loading with a highest encapsulation efficiency of 77.23% ± 5.07% at the ratio of Dex-RTA:sorafenib is 1:0.2 (Fig. S3 in Supporting information). The DL is higher when the feeding ratio is up to 1:0.4, however, the lower EE of 1:0.4 ratio recommended us to choose the 1:0.2 ratio. The DL and EE of ARS are both higher than those of ALS, indicating tighter binding force in ARS than ALS, due to the crosslinking of thioketal bond in ARS NPs.

Next, ROS-responsive property of ARS NPs was verified from multiple respects. Primarily, ROS-responsive ARS NPs disassembly was confirmed by size and morphology change. The transmission electronic microscope images revealed that the ARS NPs were spherical with a black corona at the outermost layer, indicating the successful adsorption of AMD3100, whereas after H_2O_2-treatment disruption occurred and size distribution turned into no longer uniform (Figs. 1C and D). Besides, the absence of thioketal group after H_2O_2-treatment in ^1H NMR spectrum also demonstrated the structure reorganization of ARS NPs (Fig. S2C).

When the hydrophobic thioketal group converted into hydrophilic –SH as schemed in Fig. S1 (Supporting information), the hydrophobic core was destructed, promoting the release of hydrophobic drug. So, then, the cumulative release of sorafenib in ARS NPs was detected by dialysis method. The red line in Fig. 1E showed more release of sorafenib in ARS in the presence of 1 mmol/L H_2O_2, indicating the ROS-responsive drug release of ARS NPs.

Then, the size stability of ARS NPs was investigated in PBS solution or 10% FBS solution. As shown in Fig. 1F, the particle size of ARS NPs maintained below 150 nm at least within 48 h.

As widely reported [14,27], CXCR4 is a chemokine receptor overexpressed on the cell surface of aHSCs during the progression of liver fibrosis which is induced by various cellular stress, promoting the activation of HSCs. Thus, we endowed CXCR4-targeted capability to our NPs by decorating CXCR4 antagonist AMD3100 on the surface of NPs, in order to target aHSCs more selectively in fibrotic liver. In order to verify the aHSC-targeting capacity of ARS NPs, two aspects need to be detected. First, in cellular level, the uptake in HSCs of AMD3100-modified NPs should be stronger than NPs without AMD3100-modification; second, the uptake of AMD3100-modified NPs should be stronger in fibrotic livers than healthy livers due to the higher expression of CXCR4 in fibrotic livers than healthy livers.

At first, we examined whether AMD3100 modification enhanced the intracellular uptake of nanoparticles in aHSCs. Using hydrophobic coumarin 6 (C6) as a tracer molecule, ARC (AMD-Dex-ROS-responsive-C6) nanoparticles with same characteristics as ARS nanoparticles were prepared (Fig. S4 in Supporting information). Subsequently, we found that the uptake of ARC nanoparticles modified with AMD3100 was significantly enhanced in aHSCs compared with non-targeted Dex-ROS-responsive-C6 (RC) nanoparticles (Fig. 2A, Figs. S5 and S6 in Supporting information). What is more, the uptake of ARC nanoparticles by HSCs was competitively inhibited by addition of free AMD3100 in advance, indicating that the nanoparticle targeted uptake was mediated by the CXCR4 over-expression in HSCs. Hence, the HSCs targeting *in vitro* could be proved by these results.

Then, we further detected the HSCs targeting ability of ARC NPs *in vivo* by evaluating if AMD3100-modified NPs exhibited enhanced liver uptake in CCl_4-treated mice than normal mice. All animals received humane care in compliance with the "Guide for the Care and Use of Laboratory Animals" published by the China Pharmaceutical University, and all study procedures and protocols were approved by the Animal Research Committee of China Pharmaceutical University. Chronic liver fibrosis mice model induced by continual CCl_4 intraperitoneal injection was established as portrayed

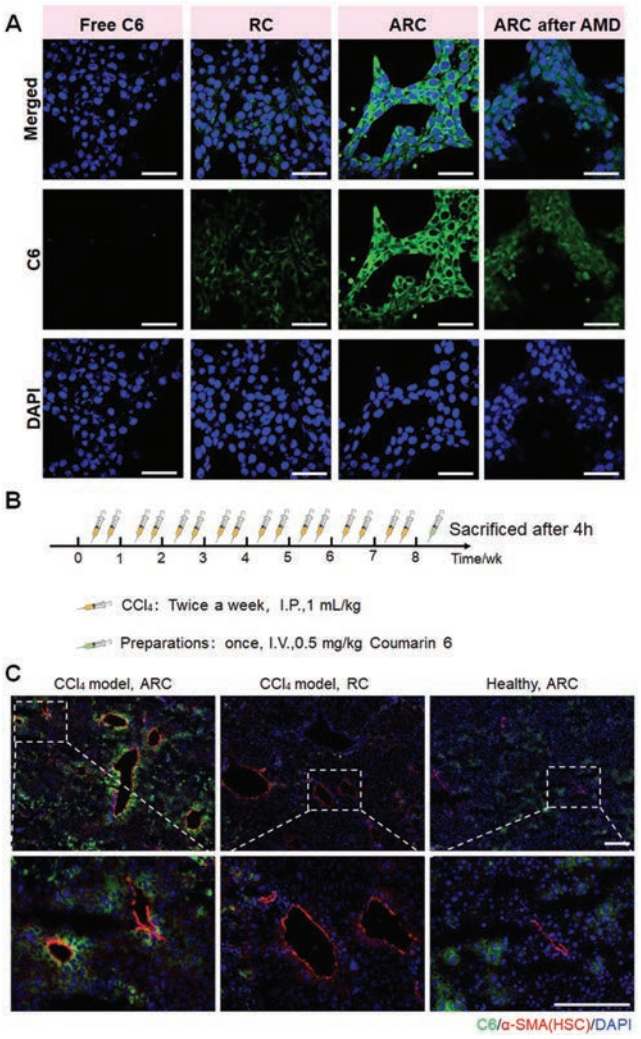

Fig. 2. The HSCs-targeting capacity of ARC (A) Cellular uptake images of free C6, RC, ARC and ARC after AMD3100-pretreatment. Scale bar = 100 μm. (B) Schematic illustration of the timeline of CCl_4 fibrosis model establishment and treatment plan. (C) The frozen liver tissue section of fibrotic mice treated with ARC and RC, and healthy mice treated with ARC. The images below are the magnifying ones of the upper ones. Scale bar = 200 μm.

in Fig. 2B, then biodistribution of C6 was detected by liver tissue immunofluorescent staining 4 h after intravenous (I.V.) injection. α-Smooth muscle actin (α-SMA) was labelled as a marker of activated HSCs. According to Fig. 2C and Fig. S7 (Supporting information), in frozen liver tissue sections of CCl_4 model mice, obvious co-localization of green C6 signal and red α-SMA signal in ARC group represented the HSCs targeting of ARC NPs. Consistently, the more tissue distribution of C6 in fibrotic liver in ARC group than normal liver was also observed according to Fig. S8 (Supporting information). Taken together, similar to the *in vitro* results, there was increased intracellular uptake of the NPs in the fibrotic livers, indicating that the CXCR4 antagonist AMD3100 can act as a targeting moiety for specific liver delivery.

Furthermore, not only as a targeting moiety, AMD3100 also exhibited strong synergistic effect with sorafenib on HSCs depletion. Firstly, the cytotoxicity of AMD-Dex-RTA vector was excluded as shown in Fig. 3A, proving the biocompatibility and biosafety of vector for various cells in liver, such as hepatocytes, macrophages and HSCs. Next, AMD3100-modified ARS NPs exerted greater cytotoxicity on activated HSCs compared with RS NPs in Fig. 3B. What is more, the addition of AMD3100 enhanced the pro-apoptosis ef-

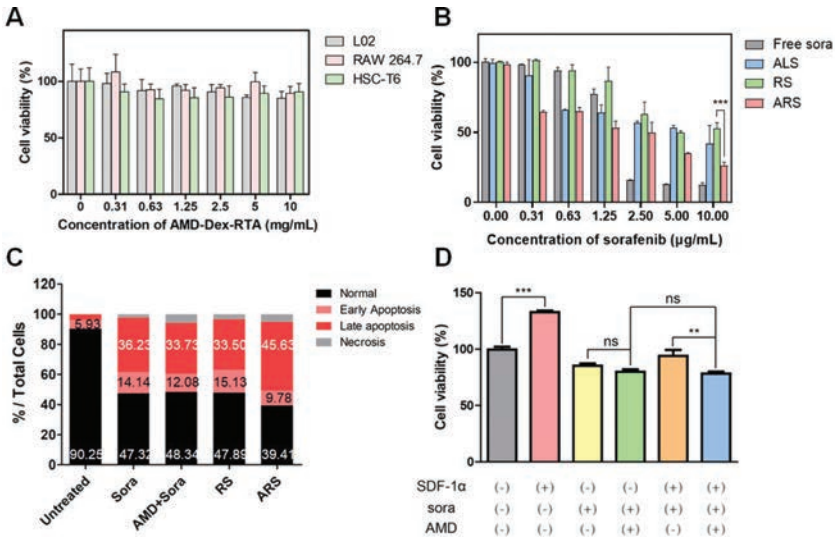

Fig. 3. (A) Cell viability of empty vector on different cells. (B) Cell viability of ARS on HSCs. (C) Cell apoptosis of ARS on HSCs. (D) Synergistic mechanism of AMD3100 on HSCs elimination. The concentrations of sorafenib and AMD3100 are both 2 μg/mL. ** $P < 0.01$, ***$P < 0.001$. ns, no significance, $P > 0.05$. Results are shown as mean ± standard deviation (SD) ($n = 5$).

fect of sorafenib on HSCs according to Fig. 3C and Fig. S9 (Supporting information), and after construction of ARS NPs, the promoting effect of AMD3100 was even stronger. Hence, AMD3100 not only enhanced HSC targeting but also magnified the sorafenib cytotoxicity on HSCs.

Next, the synergistic mechanism of AMD3100 on HSCs elimination was explored. Indeed, the sensitizing effect of AMD3100 for sorafenib treatment was probably not caused by direct cytotoxicity of AMD3100, according to the safety of AMD-Dex-RTA vector in Fig. 3A. Previous study has reported that binding of CXCR4 and its receptor SDF-1 promoted proliferation and activation of HSCs [27], probably providing protective effect for HSCs against sorafenib. To determine this, we exposed HSC-T6 cell lines to recombinant SDF-1 in advance before sorafenib treatment and explored the protective effect of SDF-1 for HSCs. We found that SDF-1 increased the viability of HSCs despite 0 μg/mL (gray *vs.* red column) or 2 μg/mL (yellow *vs.* orange column) sorafenib treatment (Fig. 3D). However, the addition of AMD3100 did not represent obviously increased HSCs cytotoxicity at the absence of SDF-1 (yellow *vs.* green column). Then, the CXCR4 antagonist AMD3100 prevented the effects of SDF-1 and sensitized HSC to sorafenib treatment (orange *vs.* blue column). Combined with the theory that CXCR4 is the unique receptor of SDF-1 [28], we could safely get the conclusion that the synergistic HSCs elimination of AMD3100 was induced by antagonizing the binding of CXCR4 and SDF-1.

Besides, ROS-responsive drug release of ARS in HSCs was explored. It is widely reported that sorafenib could induce ROS elevation in HSCs [29], so ROS level in HSCs was used as a sorafenib release indicator. As shown in Fig. S10 (Supporting information), the control HSCs group which was activated by transforming growth factor-β (TGF-β) exhibited more ROS production than the untreated group, confirmed higher ROS content in activated HSCs. Furthermore, much more ROS was produced by HSCs in ARS group than ALS group, indicating more thorough drug release of ROS-responsive nanoparticles, which demonstrated ROS-responsive drug release of ARS at the cellular level.

The above data have verified that the ARS nano-system not only enhanced the specific delivery efficiency to aHSCs, but also possessed synergetic effect on HSCs depletion. Therefore, this elaborate delivery system is promising for magnified liver fibrosis therapy. Subsequently, CCl_4-induced liver fibrosis model was used to evaluate the therapeutic efficacy of the ARS NPs. Sorafenib loaded in different formulations, were intravenously injected to mice with CCl_4-induced liver fibrosis (5 mg/kg, every other day) illustrated in Fig. 4A, and alterations of some physiological indexes reflecting hepatic function were evaluated after 4-week CCl_4 induction. Changes in hydroxyproline (Hyp) content in the liver are considered an index of collagen metabolism and provide valuable information about the severity of liver fibrosis [30]. Alanine aminotransferase (ALT) and aspartate aminotransferase (AST) are important indexes representing hepatic function and damage degree [31]. According to Figs. 4B–D, Hyp, AST and ALT levels significantly increased in CCl_4-treated mice compared with healthy mice, indicating serious liver damage in CCl_4-induced liver fibrosis. Sorafenib and AMD3100 co-delivered by final ARS NPs significantly decreased Hyp, ALT and AST compared with the model group and other treatment groups, indicating that the combination treatment may facilitate liver repair. Compared with the free drug group, the CXCR4-targeted ARS NP formulations were more effective due to the ameliorative drug delivery efficiency to aHSCs.

Next, hematoxylin & eosin (H&E), Sirius red and Masson staining were used to assess the general morphology and collagen fibers of the liver. In the healthy liver, there was normal lobular architecture, with the central vein and radiating hepatic cords (Fig. 4E). Otherwise, in the CCl_4 model group, the liver sections revealed obvious collagen fiber deposition and marked fibrosis. Marked reduction in the thickening of the collagen bundles could be observed from the Sirius red staining and Masson staining of the ARS group.

Sustained deposition of extracellular matrix mainly results from the activation of HSCs [6]. We therefore assessed the correlation between collagen accumulation and HSC activation by analyzing the expression of α-SMA, a marker of activated HSCs, in liver tissues by immumohistochemical staining and Western blot (Fig. 4F and Fig. S11 in Supporting information). The expression levels of α-SMA were markedly higher in CCl_4-treated than in healthy mice. The sorafenib alone could inhibit these pro-fibrotic factor to some extent, indicating moderate suppression of HSC activation. Excitedly, ARS delivery system combining of sorafenib plus AMD3100 significantly reduced α-SMA expression, representing the most prominent HSCs suppression and anti-fibrosis effect.

Taken together, these results confirmed that CCl_4 treatment stimulated HSCs and induced the accumulation of extracellular matrix, which may facilitate or result in liver fibrosis. The ARS drug delivery platform combining of sorafenib plus AMD3100 sig-

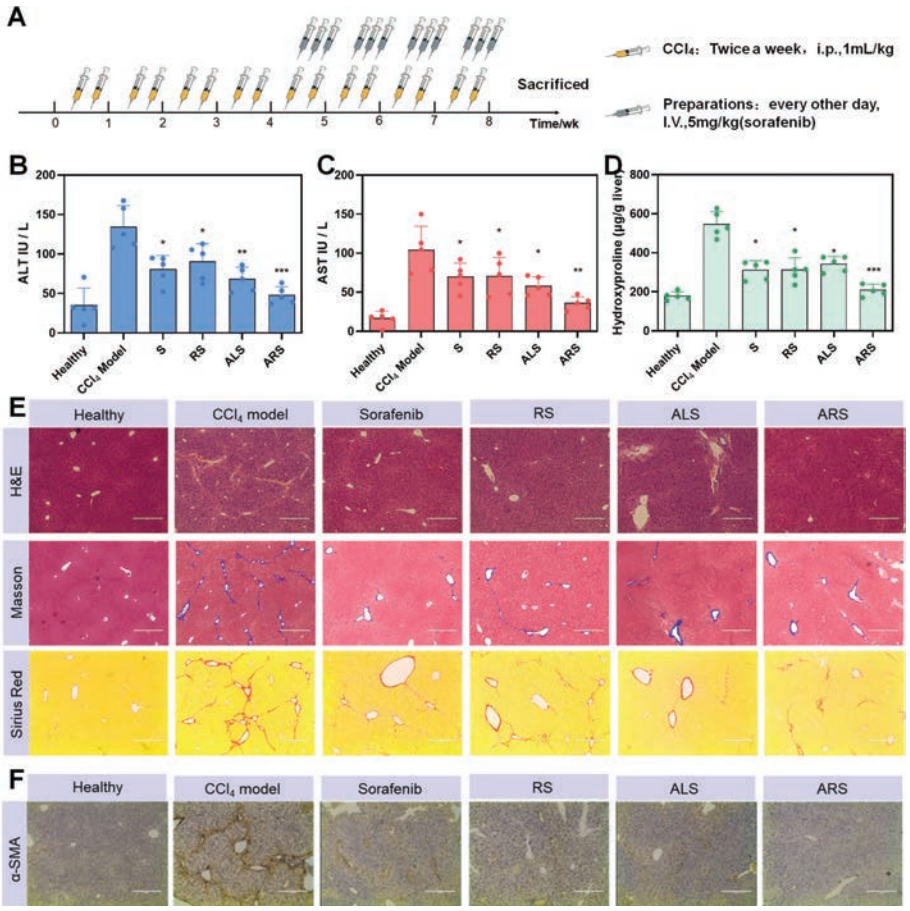

Fig. 4. Pharmaceutical effect of ARS in liver fibrosis. (A) Scheme illustration of CCl_4 model establishment and treatment. (B–D) ALT, AST and hydroxyproline content after different treatment. (E) H&E, Masson and Sirius red staining after different treatment. (F) α-SMA immunohistochemical staining after different treatment. Scale bar = 200 μm. * $P < 0.05$, ** $P < 0.01$, *** $P < 0.001$ *vs.* CCl_4 model group. Results are shown as mean ± SD ($n = 5$).

nificantly inhibited HSCs activation, induced aHSCs apoptosis and reduced liver fibrosis development.

In conclusion, we designed a CXCR4-targeted nano-system ARS NPs based on natural and biocompatible polysaccharide and thioctic acid derivative frame. By targeting CXCR4 receptor, antagonizing SDF-1/CXCR4 axis and releasing drug on demand, ARS contributed to high delivery efficiency and selective pharmacological effects to HSCs. AMD3100 as a moiety for specific HSCs-targeting and SDF-1/CXCR4-mediated HSCs protection removal, thioctic acid derivative as a ROS-responsive cross-linker, sorafenib as a main drug for promoting apoptosis of HSCs, ARS NPs displayed a satisfied anti-fibrosis effect and provided a potential research approach for anti-fibrosis system construction. In the future, deeper intracellular mechanism of the synergistic anti-fibrosis effect of AMD3100 and sorafenib could be explored and more anti-fibrosis drug could be applied in this nano platform, which is instructive for drug delivery system design and liver fibrosis clinical therapeutics.

Declaration of competing interest

The authors declare that they have no known competing financial interests or personal relationships that could have appeared to influence the work reported in this paper.

Acknowledgments

This work was financially supported by the Jiangsu Agriculture Science and Technology Innovation Fund (No. CX(22)3174), the National Natural Science Foundation of China (No. 82102202), Natural Science Foundation of Jiangsu Province (No. BK20210424) and Postgraduate Research & Practice Innovation Program of Jiangsu Province (No. KYCX23_0849).

Supplementary materials

Supplementary material associated with this article can be found, in the online version, at doi:10.1016/j.cclet.2023.108803.

References

[1] K.M. Sadek, E.A. Saleh, S.M. Nasr, Hum. Exp. Toxicol. 37 (2018) 142–154.
[2] L. Chen, J. Li, J. Zhang, et al., J. Hepatol. 62 (2015) 156–164.
[3] T. Tsuchida, S.L. Friedman, Nat. Rev. Gastroenterol. Hepatol. 14 (2017) 397–411.
[4] M. Parola, M. Pinzani, Mol. Aspects Med. 65 (2019) 37–55.
[5] F.M. Yang, H. Li, Y.M. Li, et al., Int. Immunopharmacol. 99 (2021) 108051.
[6] T. Kisseleva, D. Brenner, Nat. Rev. Gastroenterol. Hepatol. 18 (2021) 151–166.
[7] P.K. Wu, X.P. Luo, M.L. Sun, et al., Biomaterials 284 (2022) 121492.
[8] S.L. Xia, Z.M. Liu, J.R. Cai, et al., J. Control. Release 355 (2023) 54–67.
[9] W. Zhang, Y. Zhou, X. Li, X. Xu, Y. Chen, R. Zhu, et al., Biomater. Sci. 6 (2018) 1986–1993.
[10] C.T. Hung, T.H. Su, Y.T. Chen, et al., Gut 71 (2022) 1876–1891.
[11] T. Higashi, S.L. Friedman, Y. Hoshida, Adv. Drug Deliv. Rev. 121 (2017) 27–42.
[12] N.A. Luo, J.B. Li, Y.F. Chen, Drug Deliv. 28 (2021) 10–18.
[13] F. Hong, A. Tuyama, T.F. Lee, et al., Hepatology 49 (2009) 2055–2067.
[14] Y. Chen, Y. Huang, T. Reiberger, et al., Hepatology 59 (2014) 1435–1447.
[15] D.Y. Gao, T.T. Lin, Y.C. Sung, et al., Biomaterials 67 (2015) 194–203.
[16] C.H. Liu, K.M. Chan, T. Chiang, et al., Mol. Pharm. 13 (2016) 2253–2262.
[17] G. Chen, H.Z. Deng, X. Song, et al., Biomaterials 144 (2017) 30–41.
[18] T.H. Zhang, J.X. Yao, J.M. Tian, et al., Chin. Chem. Lett. 31 (2020) 1129–1132.
[19] R.D. Field, M.A. Jakus, X.Y. Chen, et al., Angew. Chem. Int. Ed. 61 (2022) e202116515.
[20] S.T. Wang, K.Y. Yu, Z.Y. Yu, et al., Chin. Chem. Lett. 34 (2023) 108184.
[21] Z.L. Zhang, S.F. Zhao, Z. Yao, et al., Redox. Biol. 11 (2017) 322–334.

[22] M. Kong, X.Y. Chen, F.Q. Lv, et al., Redox. Biol. 26 (2019) 101302.
[23] Y.M. Hao, K.C. Song, X.C. Tan, et al., ACS Nano 16 (2022) 20739–20757.
[24] Y.Y. Gao, Y. Gao, Y.F. Ding, et al., Chin. Chem. Lett. 32 (2021) 949–953.
[25] Z.H. Liu, Y.Z. Li, W. Li, et al., Adv. Mater. 30 (2018) 1703393.
[26] D. Jia, X.B. Ma, Y. Lu, et al., Chin. Chem. Lett. 32 (2021) 162–167.
[27] W.S. Zhang, R.H. Zhang, Y.Q. Ge, et al., Metabolism 135 (2022) 155271.
[28] S. Barbero, R. Bonavia, A. Bajetto, et al., Cancer Res. 63 (2003) 1969–1974.
[29] Z.L. Zhang, Z. Yao, L. Wang, et al., Autophagy 14 (2018) 2083–2103.
[30] L. Bai, Y.L. Wang, Y.L. Chen, et al., J. Clin. Periodontol. 49 (2022) 1067–1078.
[31] M.K. Halili, M.C. Shuhart, M. Lombardero, et al., Diabetes Care 41 (2018) 1251–1259.